7790 *Biochemistry* **2010,** *49,* 7790–7797
DOI: 10.1021/bi100712g

BIOCHEMISTRY
including biophysical chemistry & molecular biology
Article

Structural and Functional Characterization of the Ga-Substituted Ferredoxin from *Synechocystis* sp. PCC6803, a Mimic of the Native Protein[†,‡]

Xingfu Xu,[§] Sandra Scanu,[§] Jung-Sung Chung,[∥] Masakazu Hirasawa,[∥] David B. Knaff,[∥,⊥] and Marcellus Ubbink*[,§]

[§]*Leiden Institute of Chemistry, Leiden University, Gorlaeus Laboratories, P.O. Box 9502, 2300 RA Leiden, The Netherlands,*
[∥]*Department of Chemistry and Biochemistry, Texas Tech University, Lubbock, Texas 79409-1061, and*
[⊥]*Center for Biotechnology and Genomics, Texas Tech University, Lubbock, Texas 79409-3132*

Received May 6, 2010; Revised Manuscript Received August 2, 2010

ABSTRACT: In photosynthetic organisms, ferredoxin (Fd) interacts with many proteins, acting as a shuttle for electrons from Photosystem I to a group of enzymes involved in $NADP^+$ reduction, sulfur and nitrogen assimilation, and the regulation of carbon assimilation. The study of the dynamic interactions between ferredoxin and these enzymes by nuclear magnetic resonance is severely hindered by the paramagnetic [2Fe-2S] cluster of a ferredoxin. To establish whether ferredoxin in which the cluster has been replaced by Ga is a suitable diamagnetic mimic, the solution structure of *Synechocystis* Ga-substituted ferredoxin has been determined and compared with the structure of the native protein. The ensemble of 10 structures with the lowest energies has an average root-mean-square deviation of 0.30 ± 0.05 Å for backbone atoms and 0.65 ± 0.04 Å for all heavy atoms. Comparison of the NMR structure of GaFd with the crystal structure of the native Fd indicates that the general structural fold found for the native, iron-containing ferredoxin is conserved in GaFd. The ferredoxin contains a single gallium and no inorganic sulfide. The distortion of the metal binding loop caused by the single gallium substitution is small. The binding site on Fd for binding ferredoxin:$NADP^+$ reductase in solution, determined using GaFd, includes the metal binding loop and its surroundings, consistent with the crystal structures of related complexes. The results provide a structural justification for the use of the gallium-substituted analogue in interaction studies.

The ferredoxins found in oxygenic photosynthetic organisms, often termed plant-type ferredoxins, are reduced in the light by Photosytem I and in the dark by NADPH generated by the pentose phosphate pathway. The reduced ferredoxin (Fd)[1] serves as the electron donor for $NADP^+$ reduction, in a reaction catalyzed by ferredoxin:$NADP^+$ oxidoreductase (FNR) (*1*), and as the electron donor for a number of enzymes that play key roles in the reductive assimilation of nitrogen and sulfur (*2*, *3*). Fd also serves as the electron donor, in a reaction catalyzed by ferredoxin:thioredoxin reductase (FTR), for the reduction of thioredoxins involved in the regulation of a large number of enzymes involved in carbon assimilation and other metabolic pathways (*4*). Structural studies of formation of the complex between Fd and FNR (*1*, *5*) and between Fd and FTR (*6*) using X-ray crystallography have produced important information about the nature of these complexes. Nuclear magnetic resonance (NMR) spectroscopy has also been used to study these two complexes (*1*, *7*). However, a major limitation in the use of iron−sulfur proteins in NMR studies is the fact that fast nuclear relaxation caused by the [2Fe-2S] cluster renders the NMR resonances of the residues around the metal site invisible, although strategies for identifying and assigning resonances from nuclei near the paramagnetic center have been developed (*8*). Replacement of the paramagnetic iron−sulfur cluster with a diamagnetic metal or metal cluster provides a solution for obtaining more complete information about Fd (*9*, *10*). A previous study has shown that a colorless diamagnetic analogue of the paramagnetic Fd from *Synechocystis* sp. PCC6803, in which the paramagnetic [2Fe-2S] cluster was replaced with Ga, could be used to obtain a complete map of the binding site on Fd for FTR in solution (*7a*). The use of this approach would enable the characterization of the complexes between Fd and a variety of other enzymes. However, the replacement of the [2Fe-2S] cluster with a single metal may distort the conformation of the metal binding loop, resulting in structural differences between the GaFd and the native, iron-containing protein. Therefore, we investigated the extent of structural changes caused by the Ga substitution. The solution structure of GaFd determined by high-resolution NMR is reported. A comparison of the structures of GaFd and the native Fd shows only a small distortion in the metal loop region, whereas the general tertiary fold is well-conserved. The interaction of GaFd with FNR has been probed via NMR spectroscopy, demonstrating that the central binding site is in good agreement with the interface observed in crystal structures of the Fd−FNR complex.

[†]Support from the Chemical Sciences, Geosciences and Biosciences Division, Office of the Basic Energy Sciences, Office of Sciences, U.S. Department of Energy (Contract DE-FG03-99ER20346 to DBK), for funding the production of all of the proteins used in this study and for portions of the experimental design and interpretation of the data is gratefully acknowledged. This project was also supported by the grants from the Netherlands Organization for Scientific Research, grants 700.52.425 (M.U.), 700.58.441 (M.U.), and 700.57.011 (S.S. and M.U.) and the Volkswagenstiftung, grant I/80854 (X.X. and M.U.).

[‡]The structures and restraints have been deposited in the Protein Data Bank as entry 2KAJ. Nuclear magnetic resonance assignments have been deposited in the Biomolecular Magnetic Resonance Bank as entry 16024.

*To whom correspondence should be addressed. E-mail: m.ubbink@chem.leidenuniv.nl. Telephone: +31 71 5274628. Fax: +31 71 5275856.

[1]Abbreviations: EXAFS, extended X-ray absorption fine structure; Fd, ferredoxin; FNR, ferredoxin:$NADP^+$ oxidoreductase; FTR, ferredoxin:thioredoxin reductase; HSQC, heteronuclear single-quantum coherence; NOE, nuclear Overhauser enhancement; Pdx, putidaredoxin; TOCSY, total correlation spectroscopy.

 Published on Web 08/06/2010

MATERIALS AND METHODS

Protein Preparation and Analysis. The [2Fe-2S] ferredoxin from *Synechocystis* sp. PCC6803 was produced as described previously (*7a*). The Ga substitution and subsequent purification were performed for both ^{15}N-labeled and unlabeled Fd as reported previously (*7a*). Spinach nitrite reductase and spinach glutamate synthase were prepared as described previously (*11*, *12*). Spinach FNR was prepared according to the method of Shin and Oshino (*13*). The concentrations of the native, iron-replete Fd and of FNR were determined using published values for their extinction coefficients (*14*, *15*). The concentrations of spinach glutamate synthase and spinach nitrite reductase and of GaFd were determined according to the procedure of Bradford (*16*), using bovine serum albumin as a standard. Acid-labile sulfide was assessed using the procedure described by King and Morris (*17*), using sodium sulfide as a standard. Absorbance spectra were recorded using a Shimadzu model UV-2401 PC spectrophotometer at 1.0 nm spectral resolution.

Measurement of Complex Formation. Formation of the complex between *Synechocystis* Fd (either the native, Fe-containing Fd or GaFd) and either nitrite reductase or glutamate synthase was assessed using the previously described spectral perturbation technique (*18*). The spectra of the Fd and of the target enzyme were first measured individually, in 1.0 cm optical path length cells, and were stored in the computer interfaced with the spectrophotometer. The spectrum of the enzyme−Fd complex was then recorded under identical conditions and stored. The sum of the spectra of the two individual proteins was then subtracted from the spectrum of the complex to yield the difference spectrum resulting from complex formation. The amplitude of a selected feature in the difference spectrum was then plotted against the Fd concentration, and the data were fitted to a single binding isotherm to yield the best fit for K_d. The wavelength pairs used for measuring the spectral perturbation amplitudes were as follows: (1) 472 nm minus 400 nm for Fd and glutamate synthase, (2) 495 nm minus 390 nm for GaFd and glutamate synthase, (3) 425 nm minus 397 nm for Fd and nitrite reductase, and (4) 400 nm minus 600 nm for GaFd and nitrite reductase.

NMR Spectroscopy and Resonance Assignment. The NMR sample contained 1 mM [^{15}N]GaFd in 50 mM sodium phosphate buffer (pH 6.5) and 5% D_2O. Unlabeled 2 mM GaFd was exchanged into a 99% D_2O buffer solution by ultrafiltration using a Centriprep tube with a YM-5 membrane. All NMR spectra were recorded at 293 K, either on a Bruker DMX-600 spectrometer equipped with a TCI cryoprobe or on a Bruker 900 MHz spectrometer with a TCI cryoprobe. Backbone amides were assigned with ^{15}N−^{1}H HSQC, ^{15}N−^{1}H TOCSY-HSQC, and ^{15}N−^{1}H NOESY-HSQC (mixing time of 100 ms) conducted with a [^{15}N]GaFd sample. Water suppression in the three-dimensional (3D) experiments was achieved with the WATERGATE pulse sequence (*19*). For the side chain assignment, the unlabeled GaFd in 99% D_2O was used. High-resolution two-dimensional (2D) homonuclear TOCSY and NOESY (mixing time of 80 ms) spectra were acquired on the 900 MHz spectrometer with 1024 increments and 2048 complex data points. Water suppression was achieved with presaturation. Two TOCSY spectra with different mixing times were used to solve the ambiguity of the connectivity of protons of side chains, and the second one was also used for the analysis of H−D exchange. Aromatic ring protons were assigned on the basis of the analysis of spin systems and intra-NOEs with 2D TOCSY and NOESY spectra. NOE restraints were derived from 3D ^{15}N NOESY-HSQC and 2D NOESY spectra.

For the NMR sample in D_2O, after buffer exchange for 48 h, cross-peaks of H^N−H^α correlation of some residues can still be detected in TOCSY spectra. The amide protons of these residues were protected from deuterium exchange because they form hydrogen bonds with other atoms. In the secondary structure regions, the hydrogen bonding acceptor can be unambiguously identified. Hydrogen bond restraints were extracted for these residues and applied only in the final structure calculation. Upper distances of 2.5 and 3.3 Å were used for the H^N−O and N−O bonds, respectively.

For the study of the interaction of GaFd and FNR, in a reverse titration aliquots of a 2.2 mM solution of ^{15}N-labeled *Synechocystis* GaFd were added to a solution of 0.1 mM spinach FNR in 20 mM sodium phosphate (pH 7), 50 mM NaCl, and 6% D_2O and 2D ^{1}H−^{15}N HSQC spectra were acquired at every step on a 14.1 T NMR spectrometer. A spectrum of free GaFd was acquired under identical conditions. The chemical shift perturbations observed in the complex with 0.9 equiv of GaFd compared to free GaFd were used to determine the binding site. The average chemical shift perturbations [$\Delta\delta_{avg} = (\Delta\delta_N^2/50 + \Delta\delta_H^2/2)^{1/2}$, where $\Delta\delta_N$ and $\Delta\delta_H$ are the change in the ^{15}N and ^{1}H chemical shifts of an amide residue, respectively] were calculated.

NMR data were processed with AZARA (http://www.bio.cam.ac.uk/azara/) or NMRPipe (*20*) and analyzed with ANSIG (*21*) and CCPNMR (*22*).

Structural Calculations. For the initial structure calculation, the NOE distance restraints were generated from the manually assigned NOE peaks of the ^{15}N NOESY-HSQC spectrum. The upper distance bounds of the bins were calibrated to three categories (3.5, 4.5, and 5.5 Å) according to the peak intensities. Low-resolution structures calculated with distance restraints from ^{15}N-edited NOE spectra were further used as the starting structures for automatic assignment of cross-peaks in the 2D NOESY (mixing time of 80 ms) and ^{15}N NOESY-HSQC spectra with CYANA 2.1 (*23*, *24*). During the CYANA automatic assignment stage, the NOE distance restraints were calibrated automatically by the structure-filtered method. All long-range NOE assignments were checked manually before the final-round calculation.

To incorporate the single Ga metal into the CYANA calculation, 10 linker residues were added to connect the protein and the Ga metal. The link statement removes the van der Waals repulsions between the metal and the coordinating atoms. Extra distance restraints (2.2−2.4 Å) were also used to fix the distance from the metal to the ligands. In the final-round calculation, NOE restraints, hydrogen bond restraints for the secondary structure regions, and distance restraints for the metal were used for calculation, starting from randomized polypeptide chains. In total, 100 conformers were calculated, and the ensemble of 10 structures with the lowest target functions was used for analysis. MOLMOL (*25*) and PyMol (http://pymol.sourceforge.net/) were used to present the structures. Ramachandran plot analysis was conducted using PROCHECK-NMR (*26*). Structure calculations were performed on a Linux personal computer. The final structures and restraints have been deposited in the Protein Data Bank (PDB) as entry 2KAJ. Assignments have been deposited in the Biomolecular Magnetic Resonance Bank as entry 16024.

Docking Calculations. Docking calculations were conducted with the HADDOCK (high-ambiguity-driven biomolecular docking) server (*27*). The NMR ensemble of GaFd (PDB entry 2KAJ)

and PDB entry 1FNB (*28*) for spinach FNR were used as the inputs for docking. Only ambiguous restraints derived from chemical shift perturbation data were used to drive docking. Residues on GaFd experiencing chemical shift perturbations that are solvent accessible in free protein were defined as active residues for docking in HADDOCK. For spinach FNR, residues L94, G152, D312, and Y314, which are located around FAD, were used as active residues for docking. During the first stage of calculations, 1000 rigid body docking models were generated. The 200 lowest-energy complexes were selected for semiflexible simulated annealing, using the default protocol. The 200 lowest-energy models were then refined in water and clustered using a 2.5 Å root-mean-square deviation (rmsd) cutoff. Two top clusters (Table S2 of the Supporting Information) with the lowest HADDOCK energy scores were analyzed.

RESULTS AND DISCUSSION

Resonance Assignment. With 3D ^{15}N NOESY-HSQC and ^{15}N TOCSY-HSQC spectra, complete assignment of amide groups was achieved. With high-resolution 2D homonuclear TOCSY spectra recorded with two different mixing times and a NOESY spectrum, in combination with ^{15}N−^{1}H TOCSY-HSQC and ^{15}N−^{1}H NOESY-HSQC, almost all side chain proton resonances (95%) were assigned. For aromatic ring protons, resonances of six of the seven aromatic residues (Tyr3, Tyr37, Phe63, Tyr73, Tyr80, and Tyr96) were assigned. The nearly complete ^{1}H assignments enable the determination of a high-quality solution structure.

Solution Structure of GaFd. On the basis of a total of 2204 distance restraints (Table 1), the solution structure of GaFd was determined. The final ensemble of 10 structures with the lowest CYANA target functions has an average rmsd of 0.30 ± 0.05 Å for backbone atoms and 0.65 ± 0.04 Å for all heavy atoms. The statistics of the 10-structure ensemble are listed in Table 1, and Figure 1 presents the 10 structures superimposed. Plots of the number of restraints and rmsd per residue are provided as Supporting Information (Figures S1 and S2). The Ramachandran analysis (Table 1 and Figure S3 of the Supporting Information) displays 67.8% of the residues in the most favored region, 30.0% in additionally allowed regions, and 2.2% in generally allowed regions. The Ga-substituted Fd has a typical ferredoxin fold (Figure 2). A five-strand β-sheet and one helix form the core β-grasp of the fold. The metal binding loop and a short helix surround the core region. In the C-terminal region, a one-turn helix (E92−Y96) is not well-defined. No disulfide bond between C18 and C85 can be formed because the S^{γ} atoms of these two cysteines are separated by more than 10 Å. No long-range NOEs are observed between these two residues. In contrast, the NMR structure reported for native *Synechocystis* Fd does show a disulfide bond between C18 and C85 (*29*). However, in the crystal structure of the same native protein, no disulfide bridge is observed between C18 and C85 (*30*).

Ga Binding Site. Sulfide content analysis indicates that the GaFd contains <0.2 mol of sulfide per mole of protein, compared to the value of 2.0 mol of sulfide per mole of protein measured for the native *Synechocystis* Fd. Previous metal analysis had demonstrated that one gallium ion per protein molecule was incorporated into the protein (*7a*). An extended X-ray absorption fine structure (EXAFS) analysis of Ga-substituted putidaredoxin (Pdx) (*9*), a homologous vertebrate-type ferredoxin, suggested that the single Ga metal coordinates four cysteinyl S^{γ} atoms. On the basis of these results, it was assumed that in GaFd, a single Ga ion is coordinated by four S^{γ} atoms, one from each of the following cysteines: C39, C44, C47, and C77. Distance restraints were introduced in the structure calculations to link the Ga to these sulfur atoms. In combination with the NOE-based distance restraints, this assumption resulted in a well-defined metal binding loop (Figures 1B and 2). The coordination of the Ga metal with four S^{γ} atoms is not tetrahedral, but distorted toward square planar. A more accurate geometry determination of the metal site of GaFd will require data from other methods, such as EXAFS.

Table 1: Structural Statistics for the Ensemble of 10 Structures of GaFd

total no. of restraints	2204
no. of interproton distance restraints	2160
intraresidue	396
sequential ($\|i-j\| = 1$)	504
medium-range ($1 < \|i-j\| \leq 4$)	395
long-range ($\|i-j\| > 4$)	865
no. of H-bond restraints (two per hydrogen bond)	36
distance restraints for Ga metal	8
CYANA target function (Å^2)	1.01 ± 0.06
maximum violation for upper limits (Å)	0.12 ± 0.03
rmsd from the mean structure (Å)	
backbone atoms	0.30 ± 0.05
heavy atoms	0.65 ± 0.04
Ramachandran plot	
most favored (%)	67.8
additionally allowed (%)	30.0
generally allowed (%)	2.2
disallowed (%)	0.0

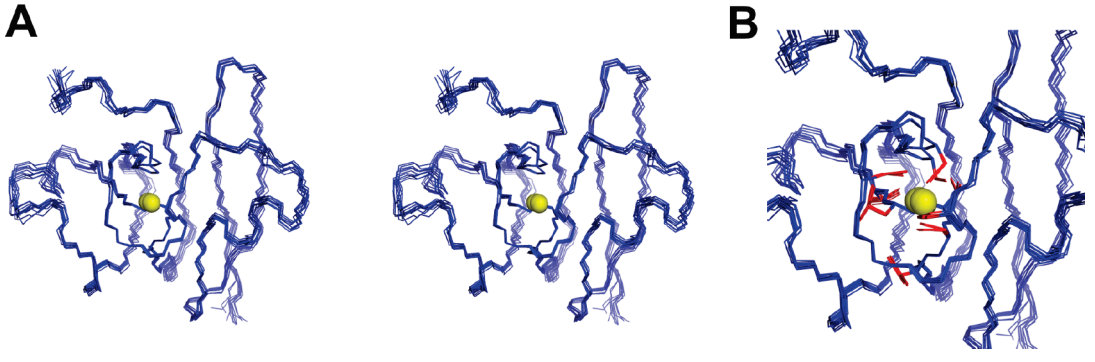

FIGURE 1: NMR structure of GaFd. (A) Stereoview of the C^{α} backbone trace of an ensemble of 10 superimposed structures of GaFd. The Gd ions are represented as yellow spheres. (B) Enlarged view of the Ga binding region. Ga ions are shown as yellow spheres, and the buried side chains of residues in the Ga binding region are shown as red sticks.

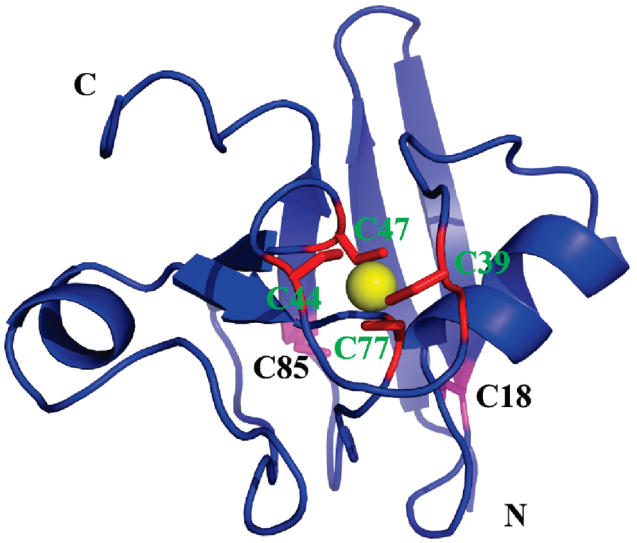

FIGURE 2: Ribbon representation of the solution structure of GaFd and the gallium metal site. The gallium metal is shown as a yellow sphere, and the four cysteine ligands are shown as red sticks. C18 and C85 are colored magenta.

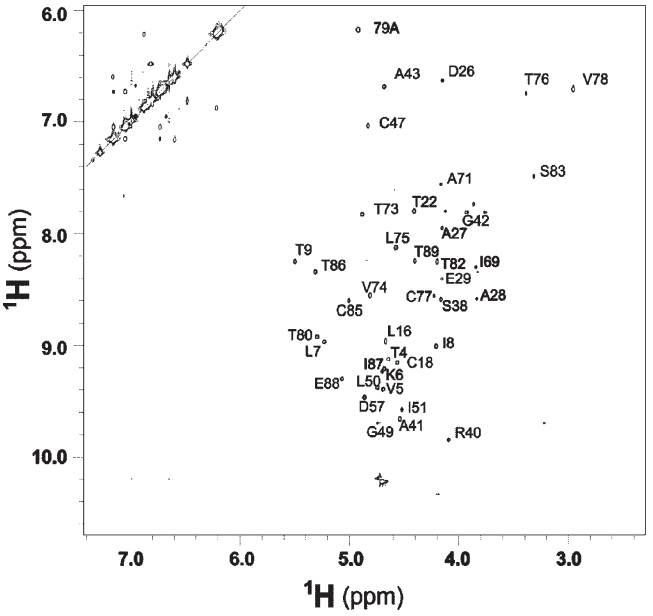

FIGURE 3: Part of a 2D homonuclear TOCSY spectrum showing the H^N-H^α correlation of residues protected from amide H−D exchange. The spectrum was recorded at 900 MHz and 293 K after incubation of protein in D_2O for 48 h.

H−D Exchange and Hydrogen Bonds. The amides of 40 residues were protected from H−D exchange after the solvent was changed to D_2O (Figure 3). As expected, most of these residues, T4−T9, I17, C19, G49−I51, and C85−E88, are in the secondary structure regions. However, residues S38 and R40−A43 are located in the metal binding loop and are solvent accessible. If the loop is dynamic, no amide signals of these residues in the loop should be visible after H−D exchange for 48 h. The fact that the residues in the loop are protected from H−D exchange, like other residues in the secondary structure regions, suggests that the amides of these residues also form intramolecular hydrogen bonds. In the native protein, the main chain nitrogens for the residues in the loop form NH-S hydrogen bonds with cysteine S^γ atoms and the sulfur atoms of the [2Fe-2S] cluster (*31*).

The number of hydrogen bonds and the strength of the hydrogen bonding network play an important role in modulating the redox potential of iron−sulfur proteins (*32*) as well as other metalloproteins (*33*). Although no hydrogen bond acceptors can be unambiguously identified on the loop for GaFd, it can be concluded that the hydrogen bond network stabilizes the Ga metal binding loop. The metal loop is thus unlikely to be very dynamic, a conclusion that is also supported by the observation of a large number of medium-range NOEs in this region.

Comparison of GaFd with Native Fd and Ga-Substituted Putidaredoxin. The solution structure of GaFd is highly similar to the crystal structure of native Fd (*30*) (Figure 4A). The rmsd of the backbone heavy atom positions between these two structures is 1.1 Å. There are small differences, mostly located in the metal binding loop. The Ga binding loop in the GaFd structure is shifted toward the α-helix formed by D66−E70, yielding a Ga position that is close to the geometrical center of the [2Fe-2S] cluster (Figure 4B).

Our data suggest a rigid metal binding loop, whereas a previous NMR study on Ga-substituted Pdx suggested that a more dynamic binding loop was generated with the incorporation of a single Ga, although the fold of the native protein was conserved (*34*, *35*). Comparison of the NMR structure of GaPdx with the recently determined crystal structure of Pdx (*36*) indicates that the distortion of the metal binding loop is relatively large. The sequence difference of the loop region for vertebrate-type and plant-type Fd may explain why a dynamic metal binding loop resulted after substitution of a single Ga for the vertebrate-type ferredoxin but not for this plant-type ferredoxin. The metal binding loop of Pdx (D-C-G-G-S-A-S-C-A-T-C) is one residue longer than that of plant-type Fd (S-C-R-A-G-A-C-S-T-C) and contains an additional Gly residue.

Formation of the Complex with Spinach Enzymes. To test whether GaFd has the same affinity for Fd-dependent enzymes as native Fd, the dissociation constant (K_d) for GaFd in complexes with two spinach enzymes that use Fd as the physiological electron donor was determined. Not surprisingly, given the very similar tertiary structures of spinach (*37*) and *Synechocystis* (*30*) ferredoxins, the native cyanobacterial protein forms complexes with spinach nitrite reductase and spinach glutamate synthase at low ionic strengths with K_d values similar to those previously observed for spinach Fd. K_d values, measured in 10 mM potassium phosphate buffer (pH 7.7), of 1.0 and 40 μM were determined for the complexes of native *Synechocystis* Fd with spinach nitrite reductase and glutamate synthase, respectively. The K_d value for spinach Fd, measured under the same conditions, was 0.7 μM in the case of nitrite reductase and 15 μM in the case of glutamate synthase. K_d values for formation of the complex of *Synechocystis* GaFd, with spinach nitrite reductase and spinach glutamate synthase, were determined to be 0.9 and 36 μM, respectively, values that are identical within the ±10% uncertainties of the measurements to those obtained using the native *Synechocystis* Fd. As the GaFd is not redox active, it was not possible to test its activity as an electron donor to these enzymes, but the observation that the affinity of GaFd for the two enzymes is identical to that observed with the native, iron-containing Fd suggests that replacement of the [2Fe-2S] cluster by Ga does not affect the interaction between Fd and the enzymes.

Binding Map of GaFd for FNR. ^{15}N-labeled GaFd was titrated into a solution of spinach FNR, and HSQC spectra were recorded at each step. Chemical shift perturbations and line broadening of the resonances were observed in comparison to

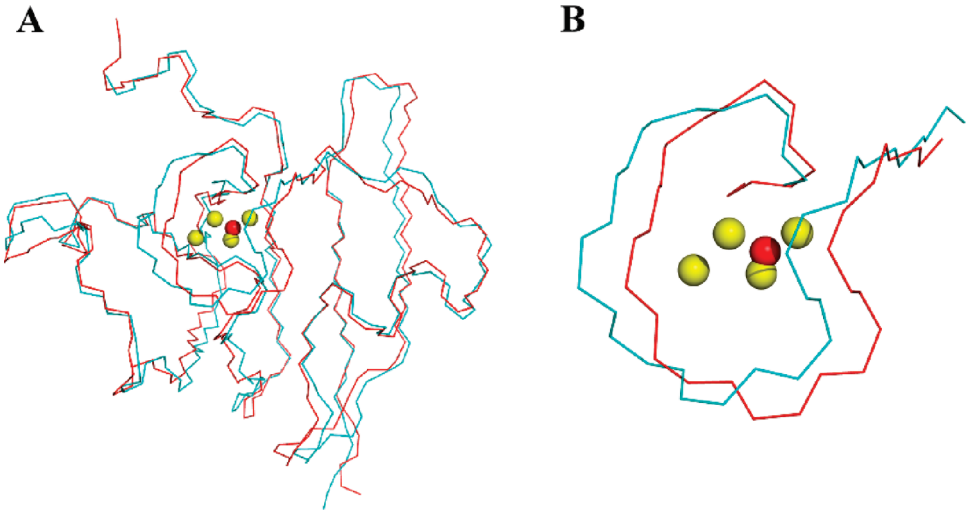

FIGURE 4: (A) Superposition of the C^{α} backbone trace of the NMR structure of GaFd (red) and the crystal structure (PDB entry 1OFF) of the native Fd (blue). The Ga metal of GaFd is shown as a red sphere, and the [2Fe-2S] cluster of Fd is shown as yellow spheres. (B) A detailed view on the metal binding sites.

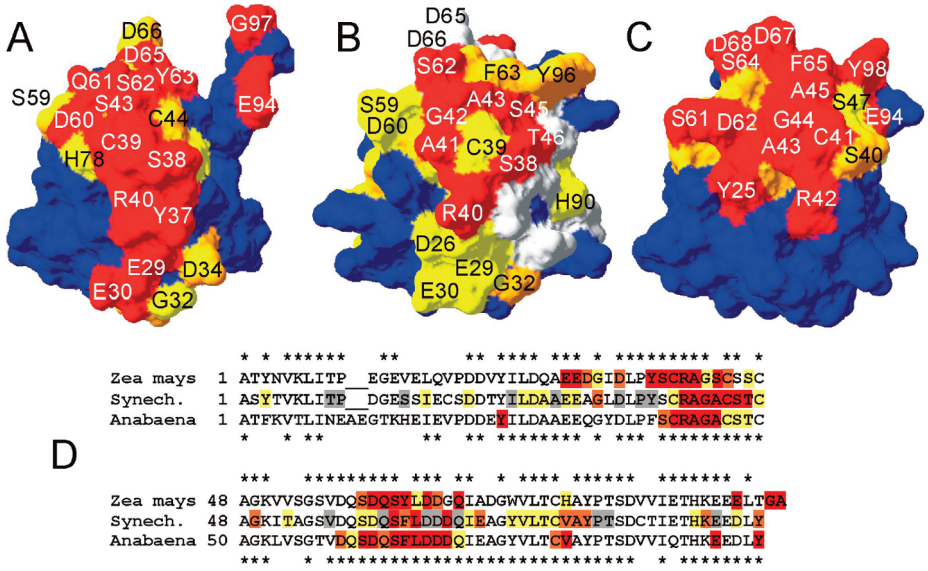

FIGURE 5: Binding site of Fd for FNR. (A and C) The structures of *Z. mays* leaf Fd [A, PDB entry 1GAQ (*1*)] and *Anabaena* PCC7119 Fd [C, PDB entry 1EWY (*39*)] are shown in surface representation and colored according to the distance from FNR observed in the crystal structures, with red, orange, and yellow for residues less than 4, 5, and 6 Å from FNR, respectively. (B) The structure of *Synechocystis* GaFd (PDB entry 2KAJ) is shown in surface representation and colored according to the chemical shift perturbations caused by binding to FNR: red for $\Delta\delta_{avg}$ (in parts per million; spectra recorded at 14.1 T) ≥ 0.100, orange for $\Delta\delta_{avg} \geq 0.050$, yellow for $\Delta\delta_{avg} \geq 0.025$, and blue for $\Delta\delta_{avg} < 0.025$. Residues with no data are colored gray. (D) Alignment of *Z. mays*, *Synechocystis*, and *Anabaena* Fd amino acid sequences, colored with the same code as in panels A−C, except that residues colored blue are shown with a white background. The asterisks indicate residues identical between *Z. mays* and *Synechocystis* (top) and *Anabaena* and *Synechocystis* (bottom).

free GaFd, indicative of binding of GaFd to FNR. In the presence of excess GaFd, the extent of perturbation and broadening decreased, toward the values for the free protein, showing that association and dissociation were fast on the NMR time scale. A binding curve (Figure S4 of the Supporting Information) indicated that the K_d is on the order of 1 μM. The chemical shift perturbations observed in the second point in the titration (Table S1 of the Supporting Information), when essentially all GaFd is bound, were mapped on the structure of GaFd (Figure 5B). The sizes of the shifts are localized and large, representative of a well-defined complex (*38*). It is clear that the loop that covers the [2Fe-2S] cluster in the native Fd (Ser38−Ser45) is located centrally in the binding site. This region is invisible in HSQC spectra of native Fd because of the paramagnetic relaxation enhancement of the cluster (*1*, *7a*), and the fact that it can be seen in the case of GaFd interacting with FNR provides further support for the utility of using the Ga-containing Fd mimic in these binding experiments. The crystal structures of the complexes of Fd and FNR from *Zea mays* (maize) (*1*) and the cyanobacterium *Anabaena* (also named *Nostoc*) PCC7119 (*5*, *39*) have been reported. The binding interfaces observed for Fd in both crystal structures are shown for comparison in panels A (maize) and C (*Anabaena*) of Figure 5. The Fd residues in the interface observed in the crystal structure are colored red, orange, and yellow, depending on their distance from FNR (less than 4, 5, and 6 Å, respectively). A comparison of panels A−C shows that the central binding site on *Synechocystis* GaFd for FNR in solution resembles the interface seen in the crystal structure for *Z. mays* Fd. Note that the numbering is different for *Anabaena* Fd because of a two-amino acid insert. Panel D presents an alignment of three Fd amino acid sequences with the same color coding.

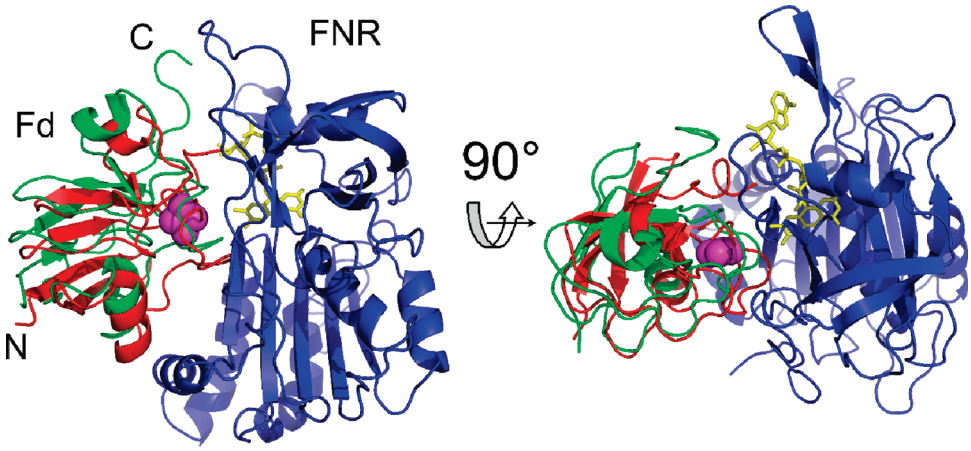

FIGURE 6: Comparison of the GaFd−FNR docking model to the crystal structure (PDB entry 1GAQ) of the maize leaf Fd−FNR complex. The FNR molecules are superimposed, and only maize leaf FNR in the complex is shown (blue ribbons). GaFd and maize leaf Fds are shown as red and green ribbons, respectively. The iron−sulfur cluster of maize leaf Fd is represented as spheres. The FAD cofactor is shown as yellow sticks.

To model the *Synechocystis* GaFd−spinach FNR complex on the basis of the chemical shift perturbation map obtained for GaFd, docking calculations were performed using the HADDOCK server (*27*). Two low-energy clusters were obtained, one of which is very similar to the maize leaf Fd−FNR crystal structure complex (Figure 6). The other cluster (Figure S5 of the Supporting Information) is very different and may represent an artifact caused by the highly ambiguous chemical shift perturbation docking restraints. In the model shown in Figure 6, the metal binding loop of GaFd docks to the concave region of FNR near the FAD cofactor, in an orientation resembling the one found in the maize Fd−FNR complex (PDB entry 1GAQ, backbone rmsd of 3.9 Å for Fd with FNR molecules superimposed). Also many intermolecular salt bridges (involving Glu29, Arg40, and Asp66 in Fd and Lys304, Glu154, and Lys88 in FNR, respectively) are found in both the cluster and the crystal structure. The *Synechocystis* GaFd−spinach FNR model is less similar to the crystal structure of the *Anabaena* Fd−FNR complex, consistent with the differences between the interface maps (Figure 5B,C).

Investigation of the interaction between Fd and FNR has not been confined to structural studies. The effects of replacement of a conserved phenylalanine (Phe65 in *Anabaena* Fd and Phe63 in *Synechocystis* Fd) suggested that the presence of an aromatic residue at this location is essential for the rapid transfer of electrons from Fd to FNR (*40*, *41*, *44*). These results are consistent with its location near the center of the interaction site on Fd for FNR determined by NMR mapping (Figure 5B) and the orientation of its side chain with respect to the [2Fe-2S] cluster and FAD prosthetic group in the X-ray structure of the *Anabaena* Fd−FNR complex (*5*, *39*). The importance of Ser47 in *Anabaena* Fd for the rapid transfer of electrons to FNR is also supported by mutagenesis experiments (*40*). This *Anabaena* Fd residue and the corresponding Ser45 in *Synechocystis* Fd can both be seen to be located in the FNR binding domains shown in the binding maps in Figure 5. In maize leaf Fd, Ser45 is close to but just outside the binding interface.

Mutagenesis experiments also suggested a crucial role in rapid electron transfer for the conserved Glu94, located in an "acidic patch" in the short C-terminal α-helix in *Anabaena* Fd (*40*, *41*, *44*). The large decreases in the rate of FNR reduction caused by charge-elimination and charge-reversal replacement of Glu94 are highly position-specific, as similar replacements at the adjacent position 95 had no effect on the electron transfer properties of the protein (*40*, *41*). In line with these results, in the crystal structure of the *Anabaena* complex, Glu94, but not Glu95, is close to FNR. However, interpreting the effects of replacing Glu94 in *Anabaena* Fd is complicated by structural effects arising from this replacement (*40*), and it also should be mentioned that the corresponding glutamate in maize leaf Fd, Glu92, is not present at the interface with maize FNR (*1*) and that charge-reversal and charge-elimination replacements of the corresponding glutamate in spinach leaf Fd produce only very modest effects on electron transfer rates (*42*, *43*). In the NMR spectrum of *Synechocystis* Fd bound to spinach FNR, the resonance of the equivalent Glu92 overlaps with another one and cannot be followed with certainty, so it is not possible to use NMR techniques to clarify the role of this conserved Fd glutamate in binding to FNR.

Another Fd acidic patch, involving Asp62, Asp67, and Asp68 (*Anabaena* numbering), has been located in the interface with FNR (*5*, *39*) in the crystal structure of this complex (also see Figure 5C). However, somewhat surprisingly, charge-reversal replacements at Asp62 and Asp68 had no effect on the rates of transfer of electrons from reduced Fd to FNR (*40*, *41*, *44*), indicating that mutagenesis experiments cannot always be used to identify amino acids involved in protein−protein interactions. The corresponding amino acids of *Synechocystis* Fd (i.e., Asp60, Asp65, and Asp66) have also been identified at the FNR binding domain in our NMR experiments (Figure 5B) and are part of the interface of maize leaf Fd for FNR (Figure 5A).

One major difference between the crystal structure of the *Anabaena* Fd−FNR complex on one hand and the NMR map of *Synechocystis* Fd and the maize leaf Fd−FNR crystal structure complex on the other is the presence of a third acidic patch in the interface in the latter two complexes. This patch involves *Synechocystis* Fd residues Gly32, Glu29, and Glu30. There is evidence that the carboxylate group of the C-terminal amino acid in Fd may be involved in an additional electrostatic interaction with FNR in both the maize leaf (*1*) and *Anabaena* (*40*, *44*). In all three maps, the C-terminal residue is part of the interface (Figure 5D).

CONCLUSIONS

The high-resolution NMR structure of GaFd from *Synechocystis* was determined. The tertiary structure of GaFd is very similar to that of native Fd. The distortion of the metal binding loop caused by Ga substitution is small, which makes the GaFd a good diamagnetic

analogue for the structural studies of the interaction of Fd with various enzymes, as was demonstrated for FNR.

ACKNOWLEDGMENT

The homonuclear TOCSY and NOESY experiments were conducted with a 900 MHz NMR spectrometer at the SON-NMR-Large Scale Facility in Utrecht. We thank Dr. R. Wechselberger for his help with the NMR experiments.

SUPPORTING INFORMATION AVAILABLE

Tables listing chemical shift perturbations and the statistics of HADDOCK docking clusters and figures presenting the per residue number of NMR restraints and rmsd, the Ramachandran plot of the NMR ensemble of GaFd, the binding curve of GaFd upon formation of the complex with FNR, and the second HADDOCK cluster. This material is available free of charge via the Internet at http://pubs.acs.org.

REFERENCES

1. Kurisu, G., Kusunoki, M., Katoh, E., Yamazaki, T., Teshima, K., Onda, Y., Kimata-Ariga, Y., and Hase, T. (2001) Structure of the electron transfer complex between ferredoxin and ferredoxin:$NADP^+$ reductase. *Nat. Struct. Biol. 8*, 117–121.
2. Hase, T., Schürmann, P., and Knaff, D. B. (2006) in Ferredoxin and ferredoxin-dependent enzymes in Photosystem I: The light-driven, plastocyanin:ferredoxin oxidoreductase (Golbeck, J. H., Ed.) pp 333−361, Kluwer, Dordrecht, The Netherlands.
3. Blankenship, R. E. (2001) It takes two to tango. *Nat. Struct. Biol. 8*, 94–95.
4. Schürmann, P., and Buchanan, B. B. (2008) The ferredoxin/thioredoxin system of oxygenic photosynthesis. *Antioxid. Redox Signal 10*, 1235–1274.
5. Morales, R., Charon, M. H., Kachalova, G., Serre, L., Medina, M., Gomez-Moreno, C., and Frey, M. (2000) A redox-dependent interaction between two electron-transfer partners involved in photosynthesis. *EMBO Rep. 1*, 271–276.
6. Dai, S. D., Friemann, R., Glauser, D. A., Bourquin, F., Manieri, W., Schurmann, P., and Eklund, H. (2007) Structural snapshots along the reaction pathway of ferredoxin-thioredoxin reductase. *Nature 448*, 92–102.
7. (a) Xu, X., Kim, S. K., Schürmann, P., Hirasawa, M., Tripathy, J. N., Smith, J., Knaff, D. B., and Ubbink, M. (2006) Ferredoxin/ferredoxin-thioredoxin reductase complex: Complete NMR mapping of the interaction site on ferredoxin by gallium substitution. *FEBS Lett. 580*, 6714–6720. (b) Xu, X. F., Schürmann, P., Chung, J.-S., Hass, M. A. S., Kim, S.-K., Hirasawa, M., Tripathy, J. N., Knaff, D. B., and Ubbink, M. (2009) The ternary protein complex of ferredoxin, ferredoxin: thioredoxin reductase, and thioredoxin studied by paramagnetic NMR spectroscopy. *J. Am. Chem. Soc. 131*, 17576–17582.
8. Machonkin, T. E., Westler, W. M., and Markley, J. L. (2004) Strategy for the study of paramagnetic proteins with slow electronic relaxation rates by NMR spectroscopy: Application to oxidized human [2Fe-2S] ferredoxin. *J. Am. Chem. Soc. 126*, 5413–5426.
9. Kazanis, S., Pochapsky, T. C., Barnhart, T. M., Pennerhahn, J. E., Mirza, U. A., and Chait, B. T. (1995) Conversion of a Fe2S2 ferredoxin into a Ga^{3+} rubredoxin. *J. Am. Chem. Soc. 117*, 6625–6626.
10. Vo, E., Wang, H. C., and Germanas, J. P. (1997) Preparation and characterization of [2Ga-2S] *Anabaena* 7120 ferredoxin, the first gallium-sulfur cluster-containing protein. *J. Am. Chem. Soc. 119*, 1934–1940.
11. Tripathy, J. N., Hirasawa, M., Kim, S. K., Setterdahl, A. T., Allen, J. P., and Knaff, D. B. (2007) The role of tryptophan in the ferredoxin-dependent nitrite reductase of spinach. *Photosynth. Res. 94*, 1–12.
12. Hirasawa, M., Chang, K. T., Morrow, K. J., and Knaff, D. B. (1989) Circular-dichroism, binding and immunological studies on the interaction between spinach ferredoxin and glutamate synthase. *Biochim. Biophys. Acta 977*, 150–156.
13. Shin, M., and Oshino, R. (1978) Ferredoxin-sepharose-4B as a tool for purification of ferredoxin:$NADP^+$ reductase. *J. Biochem. 83*, 357–361.
14. Tagawa, K., and Arnon, D. I. (1968) Oxidation-reduction potentials and stoichiometry of electron transfer in ferredoxins. *Biochim. Biophys. Acta 153*, 602–613.
15. Foust, G. P., Mayhew, S. G., and Massey, V. (1969) Complex formation between ferredoxin triphosphopyridine nucleotide reductase and electron transfer proteins. *J. Biol. Chem. 244*, 964–970.
16. Bradford, M. M. (1976) Rapid and sensitive method for quantitation of microgram quantities of protein utilizing principle of protein-dye binding. *Anal. Biochem. 72*, 248–254.
17. King, T. E., and Morris, R. O. (1964) Determination of acid-labile sulfide and sulfhydryl groups. *Methods Enzymol. 98*, 634–641.
18. Hirasawa, M., and Knaff, D. B. (1985) Interaction of ferredoxin-linked nitrite reductase with ferredoxin. *Biochim. Biophys. Acta 830*, 173–180.
19. Piotto, M., Saudek, V., and Sklenar, V. (1992) Gradient-tailored excitation for single-quantum NMR-spectroscopy of aqueous-solutions. *J. Biomol. NMR 2*, 661–665.
20. Delaglio, F., Grzesiek, S., Vuister, G. W., Zhu, G., Pfeifer, J., and Bax, A. (1995) Nmrpipe: A multidimensional spectral processing system based on unix pipes. *J. Biomol. NMR 6*, 277–293.
21. Helgstrand, M., Kraulis, P., Allard, P., and Hard, T. (2000) Ansig for Windows: An interactive computer program for semiautomatic assignment of protein NMR spectra. *J. Biomol. NMR 18*, 329–336.
22. Vranken, W. F., Boucher, W., Stevens, T. J., Fogh, R. H., Pajon, A., Llinas, P., Ulrich, E. L., Markley, J. L., Ionides, J., and Laue, E. D. (2005) The CCPN data model for NMR spectroscopy: Development of a software pipeline. *Proteins 59*, 687–696.
23. Güntert, P., Mumenthaler, C., and Wüthrich, K. (1997) Torsion angle dynamics for NMR structure calculation with the new program DYANA. *J. Mol. Biol. 273*, 283–298.
24. Herrmann, T., Güntert, P., and Wüthrich, K. (2002) Protein NMR structure determination with automated NOE assignment using the new software CANDID and the torsion angle dynamics algorithm DYANA. *J. Mol. Biol. 319*, 209–227.
25. Koradi, R., Billeter, M., and Wuthrich, K. (1996) MOLMOL: A program for display and analysis of macromolecular structures. *J. Mol. Graphics 14*, 51–55.
26. Laskowski, R. A., Rullmann, J. A. C., MacArthur, M. W., Kaptein, R., and Thornton, J. M. (1996) AQUA and PROCHECK-NMR: Programs for checking the quality of protein structures solved by NMR. *J. Biomol. NMR 8*, 477–486.
27. De Vries, S. J., van Dijk, M., and Bonvin, A. M. J. J. (2010) The HADDOCK web server for data-driven biomolecular docking. *Nat. Protoc. 5*, 883–897.
28. Bruns, C. M., and Karplus, P. A. (1995) Refined Crystal Structure of Spinach Ferredoxin Reductase at 1.7 Angstrom resolution: Oxidized, reduced and 2′-phospho-5′-AMP bound states. *J. Mol. Biol. 247*, 125–145.
29. Lelong, C., Sétif, P., Bottin, H., André, F., and Neumann, J. M. (1995) ^1H and ^{15}N NMR sequential assignment, secondary structure, and tertiary fold of [2Fe-2S] ferredoxin from *Synechocystis* sp. PCC6803. *Biochemistry 34*, 14462–14473.
30. van den Heuvel, R. H. H., Svergun, D. I., Petoukhov, M. V., Coda, A., Curti, B., Ravasio, S., Vanoni, M. A., and Mattevi, A. (2003) The active conformation of glutamate synthase and its binding to ferredoxin. *J. Mol. Biol. 330*, 113–128.
31. Fukuyama, K. (2004) Structure and function of plant-type ferredoxins. *Photosynth. Res. 81*, 289–301.
32. Lin, I. J., Gebel, E. B., Machonkin, T. E., Westler, W. M., and Markley, J. L. (2005) Changes in hydrogen-bond strengths explain reduction potentials in 10 rubredoxin variants. *Proc. Natl. Acad. Sci. U.S.A. 102*, 14581–14586.
33. Machczynski, M. C., Gray, H. B., and Richards, J. H. (2002) An outer-sphere hydrogen-bond network constrains copper coordination in blue proteins. *J. Inorg. Biochem. 88*, 375–380.
34. Kazanis, S., and Pochapsky, T. C. (1997) Structural features of the metal binding site and dynamics of gallium putidaredoxin, a diamagnetic derivative of a $Cys_4Fe_2S_2$ ferredoxin. *J. Biomol. NMR 9*, 337–346.
35. Pochapsky, T. C., Kuti, M., and Kazanis, S. (1998) The solution structure of a gallium-substituted putidaredoxin mutant: GaPdx C85S. *J. Biomol. NMR 12*, 407–415.
36. Sevrioukova, I. F. (2005) Redox-dependent structural reorganization in putidaredoxin, a vertebrate-type [2Fe-2S] ferredoxin from *Pseudomonas putida*. *J. Mol. Biol. 347*, 607–621.
37. Binda, C., Coda, A., Aliverti, A., Zanetti, G., and Mattevi, A. (1998) Structure of the mutant E92K of [2Fe-2S] ferredoxin I from *Spinacia oleracea* at 1.7 angstrom resolution. *Acta Crystallogr. D 54*, 1353–1358.
38. Worrall, J. A. R., Reinle, W., Bernhardt, R., and Ubbink, M. (2003) Transient protein interactions studied by NMR spectroscopy: The case of cytochrome *c* and adrenodoxin. *Biochemistry 42*, 7068–7076.
39. Morales, R., Kachalova, G., Vellieux, F., Charon, M. H., and Frey, M. (2000) Crystallographic studies of the interaction between the

ferredoxin:$NADP^+$ reductase and ferredoxin from the cyanobacterium *Anabaena*: Looking for the elusive ferredoxin molecule. *Acta Crystallogr. D 56*, 1408–1412.
40. Hurley, J. K., WeberMain, A. M., Stankovich, M. T., Benning, M. M., Thoden, J. B., Vanhooke, J. L., Holden, H. M., Chae, Y. K., Xia, B., Cheng, H., Markley, J. L., MartinezJulvez, M., Gomezmoreno, C., Schmeits, J. L., and Tollin, G. (1997) Structure-function relationships in *Anabaena* ferredoxin: Correlations between X-ray crystal structures, reduction potentials, and rate constants of electron transfer to ferredoxin:$NADP^+$ reductase for site-specific ferredoxin mutants. *Biochemistry 36*, 11100–11117.
41. Hurley, J. K., Salamon, Z., Meyer, T. E., Fitch, J. C., Cusanovich, M. A., Markley, J. L., Cheng, H., Xia, B., Chae, Y. K., Medina, M., Gomezmoreno, C., and Tollin, G. (1993) Amino acid residues in *Anabaena* ferredoxin crucial to interaction with ferredoxin:$NADP^+$ reductase: Site-directed mutagenesis and laser flash photolysis. *Biochemistry 32*, 9346–9354.
42. Piubelli, L., Aliverti, A., Bellintani, F., and Zanetti, G. (1996) Mutations of Glu92 in ferredoxin I from spinach leaves produce proteins fully functional in electron transfer but less efficient in supporting $NADP^+$ photoreduction. *Eur. J. Biochem. 236*, 465–469.
43. Aliverti, A., Livraghi, A., Piubelli, L., and Zanetti, G. (1997) On the role of the acidic cluster Glu 92−94 of spinach ferredoxin I. *Biochim. Biophys. Acta 1342*, 45–50.
44. Hurley, J. K., Morales, R., Martinez-Julvez, M., Brodie, T. B., Medina, M., Gomez-Moreno, C., and Tollin, G. (2002) Structure-function relationships in *Anabaena* ferredoxin/ferredoxin:$NADP^+$ reductase electron transfer: Insights from site-directed mutagenesis, transient absorption spectroscopy and X-ray crystallography. *Biochim. Biophys. Acta 1554*, 5–21.